Tight-binding calculations of stacking energies and twinnability in fcc metals

N. Bernstein[1] and E. B. Tadmor[2]

[1]*Center for Computational Material Science, Naval Research Laboratory, Washington, DC 20375, USA*

[2]*Department of Mechanical Engineering, Technion-Israel Institute of Technology, Haifa, Israel*

(Received 31 October 2003; published 29 March 2004)

We calculate the material properties needed to evaluate the tendency of a face-centered-cubic (fcc) metal to plastically deform by forming crystallographic twins as opposed to dislocation-mediated slip. We refer to this property as the *twinnability* of the metal. We use a formulation for twinnability derived from a coupling of continuum mechanics with an atomistic stress-slip relation. The essential quantities for evaluating the twinnability are elastic constants, which are measurable experimentally, and energies for various stacking sequences of the fcc (111) planes. These stacking sequences include the intrinsic stacking fault configuration as well as the unstable-stacking energy and unstable-twinning energy configurations which can only be determined computationally. We use a tight-binding model to evaluate the necessary stacking energies, as well as the extrinsic stacking fault energy and twin-boundary energy, for eight fcc metals. The accuracy of the tight-binding parameters is established by comparing them with first-principles values obtained through an extensive study of the literature. The results of the literature survey are included in the paper as a resource for the reader. We show that the ranking of these metals in order of twinnability agrees with available experimental results. We reproduce the low incidence of deformation twinning in Al, and explain it in terms of the material parameters using an approximation to the twinnability expression. We also predict that Pd, which has not been studied experimentally, should twin as easily as Cu.

I. INTRODUCTION

One of the great promises of computational methods in materials science is the ability to guide material development by predicting physical properties without empirical input. Even with advances in theoretical methods and computer power, the wide range of time and length scales involved make this a challenging goal.[1] Mechanical properties, for example, depend on processes ranging from atomic rearrangements occurring on femtosecond time scales to macroscopic deformation changing over seconds or longer. One of the most effective ways to span this gap is to develop a formulation for a macroscopic property in terms of parameters that can be computed from first principles. Such a formulation can give insight and make predictions about experimental measurements based on a limited number of atomistic calculations. In this paper we present calculations of the stacking energies needed to evaluate a predictive criterion for the mode of plastic deformation in a face-centered-cubic (fcc) metal.

Plastic deformation is essential for the useful properties of metals as structural materials. By plastically deforming under load metals dissipate energy, allowing them to be shaped and to absorb impacts without failing. Two of the most common modes of plastic deformation in fcc metals at low temperatures are slip and deformation twinning (DT).[2,3] Slip is propagated through dislocations, line defects carrying a discontinuous jump in displacement, that move through the crystal lattice leaving behind a slipped region [Fig. 1(a)]. Deformation twinning occurs when a region of crystal is transformed by the external loading into its twin (mirror) counterpart [Fig. 1(b)]. We refer to the likelihood of a material to twin, as opposed to slip, as its *twinnability*.

While DT is well known, the material parameters that control the twinnability of a material are not well understood. Even a quantitative experimental measurement of twinnability is not obvious. Two types of experiments can provide some information on this: twinning stress and twin-related texture. Twinning stress experiments measure the critically resolved shear stress on the twinning plane σ_T at the instant of twin nucleation in a sample undergoing uniaxial tension or compression. However, σ_T is probably not a material property—it depends sensitively on many factors including the purity level of the material, the grain structure, the loading orientation, and internal stress concentrations.[3] Texture is a measure of the alignment of the orientations of the crystalline grains in the material. Separating out the portion of the generated texture resulting from DT (twin-related texture) quantifies the amount of twinning occurring relative to slip. The amount of twin-related texture in cold-drawn wires of fcc metals was measured by English and Chin.[4]

Experimental observations have shown that a low intrinsic stacking fault energy (SFE) is correlated with a higher tendency to twin in fcc metals.[5] The intrinsic SFE is the energy cost per unit area for changing the local stacking of the fcc (111) planes from $ABCABC$ to $ABC|BCA$. The experimental trend is understandable, since a crystallographic twin can be thought of as a sequence of stacking faults, as shown in Fig. 2. However, it is clear that this picture is misleading, since the twinned region has locally perfect (but reversed) fcc stacking. Indeed, the experimental trend is accompanied by significant scatter. One example of particular technological interest is Al, which does not exhibit DT in bulk samples, despite having a lower intrinsic SFE than Ni and Ir, which do DT.[6] Deformation twinning in Al has only been observed near cracks in thin foils[7] and in nanocrystalline thin films under nanoindentation.[8] The failure of
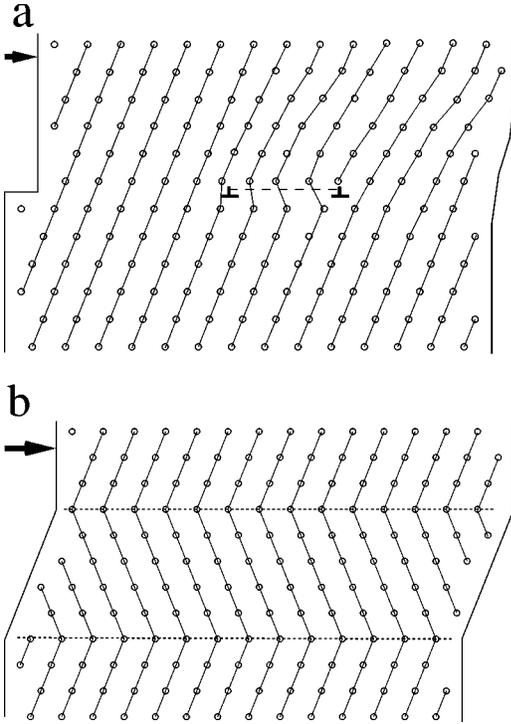
a

b

FIG. 1. Illustrations of two modes of plastic deformation. Panel (a) shows a dislocation, split into two partial dislocations bounding a stacking fault (dashed line), leading to the translation of the upper part of the crystal relative to the lower. Panel (b) shows a deformation twin bounded by mirror planes (dotted lines) created by a sequence of partial dislocations, also leading to a translation of the upper part of the crystal.

the intrinsic SFE to reliably predict twinnability strongly suggests that other factors are important for DT.

A theoretical measure for twinnability in a bulk fcc metal, based on a criterion for DT at a crack tip,[9] has recently been introduced by the authors.[10] This measure is defined in terms of elastic constants and energies for various stackings of fcc (111) planes. These stacking energies include the intrinsic SFE, as well as two energies characterizing unstable-stacking configurations described in more detail in Sec. II A. We use the tight-binding (TB) method developed at the Naval Research Laboratory[11,12] (NRL) to compute the stacking energies for eight fcc metals: Ag, Al, Au, Cu, Ir, Pb, Pd, and Pt. The TB approach's explicit description of the quantum-mechanical nature of bonding gives it a predictive power that is combined with an efficient treatment of the moderately large systems needed to compute stacking energies. Since the twinnability criterion is presented in detail elsewhere,[10] we concentrate in this paper on the TB calculations needed to evaluate the relevant material properties. We show that using these calculated values we can reproduce the experimental

A B C A B C̣B A C̣B A C̣ A B C A B C

FIG. 2. Stacking order for a twinned region, with dotted lines indicating twin boundaries and dashed lines indicating stacking faults

ranking in order of twinnability. Through an approximation to the twinnability criterion we can gain insight into the effect of the different material properties and explain the anomalous absence of DT in Al. We also predict that Pd, which has not been studied experimentally, should twin relatively easily, comparable to Cu.

In addition to the parameters required for calculating the twinnability we compute two additional stacking energies: the extrinsic SFE and the twin-boundary energy. The extrinsic SFE is analogous to the intrinsic SFE, but instead of changing the fcc stacking by removing a plane, a plane is added, changing the stacking from $ABCABC$ to $ABC|B|ABC$. The twin-boundary energy is simply the energy cost per unit area of the boundary between the normal stacking and its crystallographic twin. These energies do not enter into the twinnability measure, but they play an important role in the growth of twins and other mechanical processes, and are therefore included.

In Sec. II we briefly review the twinnability measure, and discuss the TB calculations used to evaluate the stacking energies, including the TB method, the fitting procedure used to generate parameters for the TB models, and the calculations of the stacking energies. We describe our results in Sec. III and discuss them in comparison with experiment in Sec. IV. Finally in Sec. V we present our conclusions.

II. METHOD

A. Twinnability

A criterion for DT at a crack tip was derived by Tadmor and Hai[9] based on an analysis analogous to Rice's criterion for dislocation nucleation at a crack tip.[13] The crack-tip DT criterion was validated by comparing its predictions to simulations with the quasicontinuum method using an embedded-atom empirical potential.[7] Rice's original work gave expressions for the critical stress intensity factors (SIF's) for the emission of a leading partial dislocation and a trailing partial dislocation from a crack tip. The two partials are separated by a stacking fault [see Fig. 1(a)]. The crack-tip DT criterion is determined by comparing the critical SIF for the emission of the trailing partial $K^{\perp}$ with the critical SIF for the emission of a second leading partial on a plane adjacent to the original slip plane K^{T}. The former process leads to a full dislocation, and the latter to a minimal (two layer) twinned region. The resulting expression for the twinning tendency is[9]

$$T \equiv \frac{K^{\perp}}{K^{T}} = \lambda_{\text{crit}}(\alpha, \beta, \theta, \phi, \nu, \gamma_{\text{isf}}/\gamma_{\text{us}}) \sqrt{\frac{\gamma_{\text{us}}}{\gamma_{\text{ut}}}}, \quad (1)$$

where λ_{crit} is a measure of the additional load required to emit the trailing partial of a dissociated dislocation relative to the leading partial. When $T<1$ the SIF to nucleate a trailing partial is lower than the SIF to nucleate an adjacent-plane leading partial, and slip is favored; conversely, when $T>1$ twinning is favored. The angles α, β, θ, and ϕ characterize the crystallographic orientation and loading directions. The expression for T depends on four material properties: Poisson's ratio ν, the intrinsic SFE γ_{isf}, the unstable-stacking

energy γ_{us}, and the unstable-twinning energy γ_{ut}. Poisson's ratio is an elastic constant which can be measured quite accurately. The intrinsic SFE γ_{isf} can also be measured experimentally, although typically with considerable scatter.[14] The unstable-stacking energy γ_{us} was defined by Rice to be the energy barrier to rigidly slipping one-half of an infinite crystal relative to the other half along a partial dislocation direction.[13] The unstable-twinning energy γ_{ut} is a similar quantity computed by rigidly slipping half of the crystal on a plane adjacent to a preexisting stacking fault.[9] The two unstable energies γ_{us} and γ_{ut} characterize saddle point configurations associated with energy barriers. They cannot be directly measured experimentally, but must be computed theoretically or numerically.

To relate this to deformation in the bulk we assume that the sample is polycrystalline and that there are many stress concentrators, which do not need to be microcracks. By integrating the crack-tip DT criterion over all orientations and loadings and normalizing we derive the dimensionless twinnability measure[10]

$$\tau = \frac{L}{\pi^4}\sqrt{\frac{\gamma_{us}}{\gamma_{ut}}}, \tag{2}$$

where

$$L = \int\int\int\int \lambda_{crit}(\alpha,\beta,\theta,\phi,\nu,\gamma_{isf}/\gamma_{us})d\alpha\ d\beta\ d\theta\ d\phi, \tag{3}$$

is a material property that must be computed numerically.

It can be shown that the dependence of τ on ν is weak and that an excellent approximation for Eq. (2) is given by[10]

$$\tau_a = \left[1.136 - 0.151\frac{\gamma_{isf}}{\gamma_{us}}\right]\sqrt{\frac{\gamma_{us}}{\gamma_{ut}}}. \tag{4}$$

The coefficients 1.136 and 0.151 are universal constants for the fcc lattice. It is clear from Eq. (4) that reducing the intrinsic SFE increases the twinnability of the metal, i.e., makes it more likely to twin, however the dependence of τ on the unstable energies is also clear.

B. Tight-binding calculations

To make the twinnability criterion τ predictive, we need to compute all of the necessary material specific properties without empirical input. Poisson's ratio ν can be computed from a Voigt average of the three cubic elastic constants c_{11}, c_{12}, and c_{44}, which can be easily obtained by computing the energy of a primitive fcc lattice unit cell.[15] Although we use the experimental ν here, as we mention above, the effect of ν on the twinnability is negligible. The three stacking energies γ_{isf}, γ_{us}, and γ_{ut} can be computed by comparing the energy of a system with the appropriate stacking sequence to the perfect crystal. We use the TB method to compute these quantities. With a minimal-basis description of the quantum-mechanical nature of the electrons that mediate interatomic

bonding, the TB approach combines transferability and computational efficiency that makes it possible to predict unstable stacking energies.

We use the NRL-TB method, which uses a nonorthogonal basis with on-site orbital energies that depend on the local atomic environment.[11,12] In the nonorthogonal TB approach the electrons that mediate bonding are described by a Hamiltonian and overlap matrix, with the matrix elements between orbitals of two atoms written explicitly as a function of the relative positions of the two atoms. In the NRL-TB method the angular dependence of the off-diagonal matrix elements is given by the Slater-Koster two-center form, and the distance dependence is parametrized to fit first-principles calculations as described below. The on-site matrix elements are a function of the local atomic environment. The total energy is given by the sum of the occupied eigenstates of the Hamiltonian. For most of the elements the Hamiltonian and overlap matrices are written in an sp^3d^5 basis with nine orbitals per atom. The one exception is Pb, where an sp^3 basis with four orbitals per atom is sufficient.

The original NRL-TB models were derived by fitting the energy bands and total energies of several high-symmetry bulk structures to first-principles density-functional-theory calculations. For the fcc metals we are interested in (Ag, Al, Au, Cu, Ir, Pb, Pd, and Pt), these structures include fcc and body-centered cubic, as well as additional structures such as simple cubic and diamond structure for some elements.[12] As an initial point for our calculations we use the parametrizations used by Mehl *et al.* to compute γ_{isf} and γ_{us}.[16] While experimental measurements and NRL-TB parametrizations for Ni are also available, our implementation of the TB simulation program did not include support for ferromagnetic materials.

To compute the stacking energies we create periodic supercells in a slab geometry, with 20 $(11\bar{1})$ layers, each containing one atom with $\frac{1}{2}[101]\times\frac{1}{2}[011]$ periodicity in plane. To sample the Brillouin zone (BZ) of the slab supercell we use a mesh of $34\times34\times2$ k points in reciprocal space aligned with the reciprocal lattice vectors. An equivalent density of points converges the bulk lattice constant to about 0.01%, and the bulk energy to about 1 meV/atom. All slab supercell calculations are carried out at the TB equilibrium lattice constant.

For the calculation of γ_{isf} and γ_{us} the layers are initially arranged in fcc stacking except for two twin boundaries ten layers apart, as shown in Fig. 3(a). This initial configuration is relaxed by minimizing the energy using a conjugate gradient algorithm[17] with respect to atomic displacements along the $[11\bar{1}]$ direction, and with respect to the unit cell size along the $[11\bar{1}]$ direction. The positions are relaxed until the root-mean-squared force is less than 0.0022 eV/Å and the normal virial is less than 0.01 eV. For Cu, for example, this tolerance on the virial corresponds to a stress of less than 4.6×10^{-5} eV/Å^3=7 MPa.

To create a stacking fault, a slab of nine layers surrounding one of the twin boundaries is moved along the [112] direction. The slab is moved in 20 $\frac{1}{20}a\sqrt{\frac{3}{2}}$ steps, where a is the lattice constant. At each step the system is relaxed as

(a)

(b)

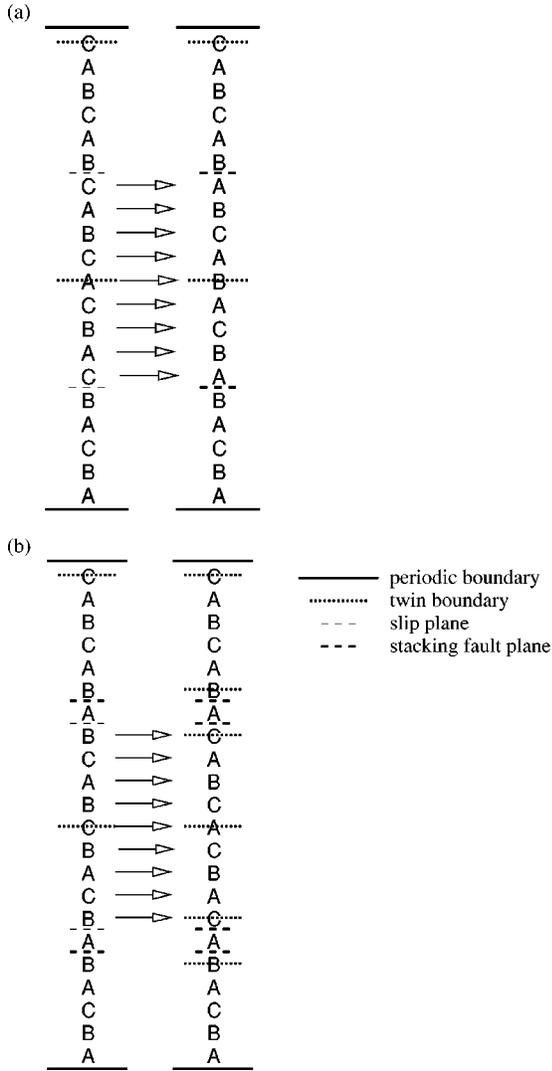| | periodic boundary |
....	twin boundary
- - -	slip plane
-- --	stacking fault plane

FIG. 3. Schematic representations of the unit cells used to calculate the stacking energies, with the fcc (111) stacking order indicated by the letters A, B, and C. Panel (a) shows the initial and final configurations of the supercell for computing γ_{isf} and γ_{us}, and panel (b) shows the initial and final configurations for computing γ_{ut}.

described above. At the final step two intrinsic stacking faults are formed, and the difference between the initial and final relaxed energies is twice γ_{isf}. The maximum energy point along the path determines γ_{us}. The calculation of γ_{ut} is similar, except for the slab which initially consists of 22 layers, with two twin boundaries and two stacking faults [see Fig. 3(b)]. The translated slab is adjacent to the two stacking faults, as shown in Fig. 3(b), consistent with the definition of γ_{ut}. At the end of the translation, two extrinsic stacking faults are formed.

We found that the relaxed γ_{isf} computed using the published parametrizations was not sufficiently accurate for our purposes: The ranking in order of intrinsic SFE did not agree with experiment (see Table I). To fix this we added an unrelaxed intrinsic stacking fault configuration to the fitting database for Ag, Cu, Ir, and Pb. For the fitting energy we took

a value close to the high end of the range of experimental values, although experimental measurements are of course relaxed. Since we were not concerned with an exact fit but rather with a reasonable reproduction of the experimental ordering and energy scales, this approach was sufficient. The resulting parameters did not noticeably change the fit of the original bulk structure fitting database, indicating that the original fitting problem is somewhat underconstrained. The new parameter sets are listed in Appendix A. While the intrinsic SFE for these four elements can no longer be considered a prediction of the TB model, the two experimentally inaccessible quantities γ_{us} and γ_{ut}, as well as the extrinsic SFE and twin boundary energy, still are.

III. RESULTS

The results of our stacking energy calculations are plotted in Fig. 4. The different fcc metals show different behaviors. The overall range of energies is wide, from about 100 to almost 1000 mJ/m^2, reflecting the general trend of decreasing ductility from Ag to Ir. The shapes of the curves vary as well. The positions of the maxima are mostly half way between stable configurations, although exceptions such as Al are noticeable. The relative heights of the two unstable-stacking-energy maxima and the intrinsic SFE minimum, which control the twinnability, vary significantly among the eight metals.

The relevant energies are listed in Table I. We list the quantities needed for computing τ: γ_{isf}, γ_{us}, and γ_{ut}, as well as the extrinsic SFE γ_{esf} and twice the twin-boundary energy $2\gamma_t$. The table includes the results for the original NRL-TB parametrization along with our parametrizations for Ag, Cu, Ir, and Pb. The set of TB parametrizations we use for the twinnability calculations (referred to as the current parametrization set) is comprised of Ag^n, Al, Au, Cu^n, Ir^n, Pb^n, Pd, and Pt. The TB results are compared with experimental data and first-principles (FP) calculations. It is clear from the range of the experimental and FP values that these quantities are difficult to determine accurately. The average uncertainty, across all parameters, in the experimental results is $\pm 17.7\%$ and in the FP results $\pm 21.6\%$.

To evaluate the accuracy of the TB results, we present in Table II the average relative deviations between the FP values and experiment, the TB values and experiment, and the TB and FP values. We note that the agreement between the TB results and experiment is comparable to the agreement between the FP results and experiment. In fact, for the intrinsic SFE, the current set of TB parametrizations gives better agreement with experiment than the FP calculations. The reason for this is that these parametrizations include the intrinsic SFE as a fitted quantity. The overall agreement between TB and FP is about 30% for the stacking energies and 24% for the unstable stacking energy. This agreement is comparable to the accuracy of the first-principles results themselves.

Crampin et al.[18] noted in their first-principles calculations that due to small long-range interactions, stacking energies are generally proportional to the number of faults. Thus, the relation $2\gamma_t \approx \gamma_{isf} \approx \gamma_{esf}$ is expected to hold, with the intrinsic SFE normally a little higher than the extrinsic SFE. This

TABLE I. Stacking energies for fcc metals in mJ/m^2: intrinsic SFE γ_{isf}, extrinsic SFE γ_{esf}, twice the twin-boundary energy $2\gamma_t$, unstable-stacking energy γ_{us}, and unstable-twinning energy γ_{ut}. Listed values include a range of published data (listed in detail in Appendix B) from experiment (expt.) and from first-principles calculations (FP), as well as our tight-binding work (TB). Results from the new parametrizations are indicated with a superscript "n."

Mat.	γ_{isf}^{expt}	γ_{isf}^{FP}	γ_{isf}^{TB}	γ_{esf}^{expt}	γ_{esf}^{FP}	γ_{esf}^{TB}	$2\gamma_t^{expt}$	$2\gamma_t^{FP}$	$2\gamma_t^{TB}$	γ_{us}^{FP}	γ_{us}^{TB}	γ_{ut}^{TB}
Ag^n	18±3	35±15	18		33±5	20	16	33±5	25	190	93	105
Ag		36				39			43		123	143
Al	167±33	203±77	99	180	184±76	94	195±45	185±75	83	199±25	164	207
Au	37±8	44	49		44	52	30	42	52		110	135
Cu^n	61±17	54±16	64		63±10	65	48	64±8	60	184±26	200	236
Cu		30				32			33		182	202
Ir^n	390±90	474±60	305		494	260		486	257	910	679	872
Ir			555			523			526		691	957
Pb^n	25		30			31	20		12		98	108
Pb		63				72			76		108	143
Pd	177±3	168±8	107		167±11	102	165±13		112	265	313	355
Pt		322	270			316	322		60		388	521

relation is satisfied to reasonable accuracy by all of the TB parametrizations with the exception of Pt and the parametrization for Pb. For Pb, the experimental values suggest that the calculated intrinsic and extrinsic SFEs are a little high and the twin-boundary energy is a little low. For Pt, the calculated intrinsic SFE is a little too low and the twin-boundary energy is dramatically too low. The reasons for these deviations, and in particular for the very low twin-

boundary energy for Pt, are not clear. However, errors in twin-boundary energy will not affect the evaluation of twinnability discussed next. In their calculations, Crampin *et al.* also found that on average the intrinsic SFE is larger than the extrinsic SFE by 7.7%. Discounting Pt with its too low intrinsic SFE, we find similarly that the intrinsic SFE is larger than the extrinsic SFE by 7.9% on average.

The twinnability of the fcc metals we studied is listed in Table III. We include results of experimental twinning stress, twin-related texture, a numerically integrated evaluation of τ from Eq. (2), and τ_a from Eq. (4). The twinnabilities τ and τ_a are computed using the TB stacking energies and the experimental Poisson's ratio (only used in τ). From the two experimental measures we can determine the following ranking in order of increasing twinning tendency:

$$Al < Ir < (Au)_f < Ni < Cu < Pb < (Au)_\sigma < Ag. \qquad (5)$$

The two measures are consistent except for the ranking of Au, which we label by $(Au)_f$ for the twin-related texture ranking and by $(Au)_\sigma$ for the twinning stress ranking. We place Al below Ir because while there are numerous examples of DT in Ir,[19-21] Al does not twin as described in Sec. I. The theoretical twinnability measure τ gives a ranking of
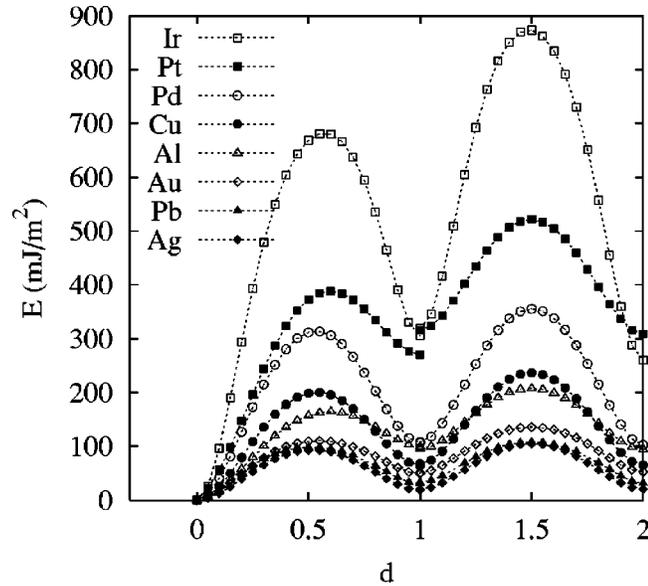
$$Pt < Al < Ir < Au < Cu < Pd < Pb < Ag, \qquad (6)$$

FIG. 4. Energy as a function of total fractional displacement for each element, starting with displacement corresponding to the formation of an intrinsic stacking fault $0 \leq d \leq 1$, followed by the displacement corresponding to the formation of an extrinsic stacking fault $1 \leq d \leq 2$. The unstable-stacking structure is at $d \approx 0.5$, intrinsic stacking fault at $d = 1.0$, unstable-twinning fault at $d \approx 1.5$, and the extrinsic stacking fault at $d = 2.0$. The small discontinuity at $d = 1.0$ reflects the difference between the 20 and 22 layer slabs caused by incomplete convergence with respect to slab thickness and BZ sampling.

TABLE II. Average relative deviation (%) for the listed material parameters between FP and experiment, TB and experiment, and TB and FP. For the TB values the numbers outside the parentheses are for the current set of parametrizations and the numbers in parentheses for the original parametrizations.

	γ_{isf}	γ_{esf}	$2\gamma_t$	γ_{us}
FP vs expt.	29.3		46.1	
TB vs expt.	22.8 (65.4)		52.2 (97.6)	
TB vs FP	31.1 (24.6)	32.7 (29.9)	31.3 (33.2)	24.2 (19.2)

TABLE III. Twinnability measures from experiment and our calculations. Experimental measures are twinning stress σ_T (MPa) and fraction of twin-related texture f (%). Twinning stress results are listed as the range of observed values listed in detail in Appendix B. The twinnability measure τ and approximate twinnability measure τ_a are unitless.

Mat.	σ_T	f	τ	τ_a
Ag	65.5 ± 25.5	95 ± 5	1.044	1.042
Pb	105 ± 60		1.040	1.038
Pd			1.020	1.018
Cu	110 ± 70	34	1.001	1.001
Ni	300	27		
Au	90 ± 10	16	0.965	0.965
Ir	1000		0.943	0.943
Al			6.5 ± 1.5	0.930	0.930
Pt			0.892	0.890

TABLE IV. Parameters for NRL-TB Ag Hamiltonian in the notation of Ref. 28.

On-site parameters				
λ	1.2249			
Orbital	a (Ry)	b (Ry)	c (Ry)	d (Ry)
s	0.1715	8.3847	-17.2341	0.0000
p	0.6054	12.3508	21.0041	0.0000
d	0.0043	0.0860	-0.5580	0.0000

Hamiltonian matrix parameters				
Interaction	e (Ry)	f (Ry/a.u.)	g (Ry/a.u.^{2})	h (a.u.$^{-1/2}$)
$H_{ss\sigma}$	-3.0391	0.2734	0.0000	0.7539
$H_{sp\sigma}$	2.4618	-0.0673	0.0000	0.7936
$H_{pp\sigma}$	-15.2682	4.5479	0.0000	0.8991
$H_{pp\pi}$	-1241.6549	103.5693	0.0000	1.7147
$H_{sd\sigma}$	-1.1265	0.0945	0.0000	0.7072
$H_{pd\sigma}$	3.7277	-1.4888	0.0000	0.9002
$H_{pd\pi}$	2.2826	0.0992	0.0000	1.0413
$H_{dd\sigma}$	-3.0612	-0.6645	0.0000	0.9771
$H_{dd\pi}$	9.7425	-0.8077	0.0000	1.0155
$H_{dd\delta}$	28.7825	-13.0338	0.0000	1.3706

Overlap matrix parameters				
Interaction	p (a.u.$^{-1}$)	q (a.u.$^{-2}$)	r (a.u.$^{-3}$)	s (a.u.$^{-1/2}$)
$S_{ss\sigma}$	5.1571	-0.1874	0.0000	0.8604
$S_{sp\sigma}$	-2.3772	-0.1850	0.0000	0.7744
$S_{pp\sigma}$	-3.7611	-0.5032	0.0000	0.9064
$S_{pp\pi}$	-5483.6580	1301.8405	0.0000	1.3654
$S_{sd\sigma}$	0.2886	0.0328	0.0000	0.7242
$S_{pd\sigma}$	-7.1302	2.6584	0.0000	0.9526
$S_{pd\pi}$	-1.8137	0.2638	0.0000	0.7566
$S_{dd\sigma}$	14.0832	-2.5248	0.0000	0.9447
$S_{dd\pi}$	-7.9469	0.2773	0.0000	1.0472
$S_{dd\delta}$	33.5650	-10.7158	0.0000	1.1595

TABLE V. Parameters for NRL-TB Cu Hamiltonian in the notation of Ref. 28.

On-site parameters				
λ	1.4564			
Orbital	a (Ry)	b (Ry)	c (Ry)	d (Ry)
s	0.0286	60.7425	-5801.5500	220027.8101
p	0.3390	88.8634	-6288.1282	176181.3499
d	-0.0029	-2.7834	439.8528	-13354.9851

Hamiltonian matrix parameters				
Interaction	e (Ry)	f (Ry/a.u.)	g (Ry/a.u.^{2})	h (a.u.$^{-1/2}$)
$H_{ss\sigma}$	-5.5681	1.6333	-0.4423	0.9684
$H_{sp\sigma}$	1.4289	0.1135	0.0214	0.8157
$H_{pp\sigma}$	-0.7219	0.6779	-0.0324	0.7706
$H_{pp\pi}$	-0.2720	-1.6311	0.2893	0.9186
$H_{sd\sigma}$	-0.4868	-0.1222	-0.0278	0.9259
$H_{pd\sigma}$	-0.2936	-0.0722	0.0013	0.7427
$H_{pd\pi}$	-1.7962	0.8572	0.1392	1.0456
$H_{dd\sigma}$	-2.6746	0.6147	-0.0343	0.7956
$H_{dd\pi}$	7.6177	-1.7022	0.1236	1.0069
$H_{dd\delta}$	-0.2164	-0.1560	-0.0614	1.0926

Overlap matrix parameters				
Interaction	p (a.u.$^{-1}$)	q (a.u.$^{-2}$)	r (a.u.$^{-3}$)	s (a.u.$^{-1/2}$)
$S_{ss\sigma}$	-1.7966	1.0111	0.2955	0.9633
$S_{sp\sigma}$	34.9588	-13.0188	0.6087	0.9870
$S_{pp\sigma}$	47.0517	-15.0274	0.4065	1.0306
$S_{pp\pi}$	-45.2743	21.2989	-2.2218	0.9728
$S_{sd\sigma}$	1.8783	-1.0250	0.0327	1.1319
$S_{pd\sigma}$	1.1845	-0.7127	-0.3112	1.0760
$S_{pd\pi}$	-8.2648	0.7368	0.0209	1.0207
$S_{dd\sigma}$	5.7560	0.1723	-0.2743	1.0148
$S_{dd\pi}$	-8.6622	0.3814	0.5494	1.2074
$S_{dd\delta}$	0.1331	-0.2943	0.0784	0.9834

in agreement with the experimental ranking using the twin-related-texture measure for Au.

To gauge the effect of the TB error on the twinnability predictions we consider the error in the ratio $\gamma_{\text{isf}}/\gamma_{\text{us}}$ upon which twinnability depends (the error in the ratio $\gamma_{\text{us}}/\gamma_{\text{ut}}$ cannot be evaluated since FP results for the unstable-twinning energy are not available). The average deviation between TB and FP is 26.8%.[22] Neglecting the error in $\sqrt{\gamma_{\text{us}}/\gamma_{\text{ut}}}$ (Ref. 23) the maximum and minimum values for the twinnability from Eq. (4) are

$$\tau_a^{\min} = [1.136 - 0.151(1+\epsilon)g] \sqrt{\frac{\gamma_{\text{us}}}{\gamma_{\text{ut}}}},$$

$$\tau_a^{\max} = [1.136 - 0.151(1-\epsilon)g] \sqrt{\frac{\gamma_{\text{us}}}{\gamma_{\text{ut}}}}, \tag{7}$$

where $g = \gamma_{\text{isf}}/\gamma_{\text{us}}$ and ϵ is the typical error in g. The relative error in twinnability is then

$$(\tau_a^{\min} - \tau_a)/\tau_a = -0.151\epsilon/(1.136 - 0.151g),$$

TABLE VI. Parameters for NRL-TB Ir Hamiltonian in the notation of Ref. 28.

On-site parameters			
λ	1.4884		
Orbital	a (Ry)	b (Ry)	c (Ry)	d (Ry)
s	0.2703	95.9250	−4247.4716	−271016.4612
p	0.6429	125.3454	9083.2794	131963.6858
d	0.0583	0.6588	218.0724	−22557.5909

Hamiltonian matrix parameters			
Interaction	e (Ry)	f (Ry/a.u.)	g (Ry/a.u.^{2})	h (a.u.$^{-1/2}$)
$H_{ss\sigma}$	−1.2866	−0.1142	−0.0016	0.8144
$H_{sp\sigma}$	1.7556	0.5706	−0.0016	0.8466
$H_{pp\sigma}$	1.2729	1.0542	0.0023	0.8303
$H_{pp\pi}$	192.5692	−41.4208	0.0544	1.1381
$H_{sd\sigma}$	−2.9749	0.3208	−0.0048	0.7852
$H_{pd\sigma}$	1.8261	−0.6489	−0.0017	0.8274
$H_{pd\pi}$	1.0552	−0.0604	0.0029	0.8222
$H_{dd\sigma}$	−1.7256	−0.3260	−0.0023	0.8656
$H_{dd\pi}$	4.4714	−0.0413	0.0350	0.9368
$H_{dd\delta}$	−0.9373	0.0982	−0.0015	0.8338

Overlap matrix parameters			
Interaction	p (a.u.$^{-1}$)	q (a.u.$^{-2}$)	r (a.u.$^{-3}$)	s (a.u.$^{-1/2}$)
$S_{ss\sigma}$	8.1003	−1.3087	0.0028	0.8834
$S_{sp\sigma}$	1907.9810	−538.4131	6.7154	1.4135
$S_{pp\sigma}$	5851.0632	−6938.2576	1077.0171	1.5473
$S_{pp\pi}$	696.9628	−136.6318	0.4710	1.2257
$S_{sd\sigma}$	−1.3139	0.4873	−0.0001	0.7332
$S_{pd\sigma}$	0.9721	−0.0648	−0.0001	0.5194
$S_{pd\pi}$	−1.2268	0.4554	0.0036	0.8802
$S_{dd\sigma}$	0.8247	−0.0155	0.0007	0.7182
$S_{dd\pi}$	−3.4569	−0.0556	−0.0094	0.8882
$S_{dd\delta}$	138.8453	−4.2736	−4.3770	1.1991

TABLE VII. Parameters for NRL-TB Pb Hamiltonian in the notation of Ref. 28.

On-site-parameters			
λ	1.0715		
Orbital	a (Ry)	b (Ry)	c (Ry)	d (Ry)
s	−0.3457	4.6131	−43.6552	−760.9337
p	0.4666	−1.0573	−106.0625	2305.8282

Hamiltonian matrix parameters			
Interaction	e (Ry)	f (Ry/a.u.)	g (Ry/a.u.^{2})	h (a.u.$^{-1/2}$)
$H_{ss\sigma}$	−19.7480	−1.5860	−0.1731	1.0024
$H_{sp\sigma}$	−22.7677	11.4624	−2.2656	1.0327
$H_{pp\sigma}$	−6.4979	−0.6030	0.8579	0.9708
$H_{pp\pi}$	−0.6946	0.3947	−0.0639	0.9300

Overlap matrix parameters			
Interaction	p (a.u.$^{-1}$)	q (a.u.$^{-2}$)	r (a.u.$^{-3}$)	s (a.u.$^{-1/2}$)
$S_{ss\sigma}$	140.7587	−22.3809	0.8875	0.9892
$S_{sp\sigma}$	59.6957	2.8046	−0.1521	0.9906
$S_{pp\sigma}$	−26.9853	18.6299	−3.7955	0.9794
$S_{pp\pi}$	7.4559	−4.4049	0.7728	0.9538

$$(\tau_a^{\max} - \tau_a)/\tau_a = 0.151\epsilon/(1.136 - 0.151g). \qquad (8)$$

The upper bound on the error is obtained for $g = 1$ when the denominator is minimal. For $\epsilon = 26.8\%$ the maximum error in twinnability is 4%. This is a low value which suggests that the accuracy of the TB calculations is sufficient for the present analysis. Errors in the TB parameters may affect the ordering according to twinnability of some neighboring materials, but will not affect our main conclusions.

IV. DISCUSSION

The agreement in the ranking of the fcc metals according to the experimental and theoretical twinnabilities validates our expression for τ and shows that the TB approach is sufficiently accurate for computing stacking energies that enter into τ. In particular, the agreement with the texture related ranking for Au is expected. From Eq. (1) it is clear that T is a measure of whether a particular slip system will twin or slip, so τ as the orientational average of T is a measure of the number and strength of active twinning systems in a polycrystal. It is reasonable that a material with more active twin-

ning systems will produce more twin-related texture upon mechanical deformation.

As Table III shows, the approximation for τ in Eq.(4) is accurate to about 0.2%. This result makes it straightforward to compute the twinnability of a material without any experimental input, since τ_a depends only on the three stacking energies. Using a first-principles method or a TB model fit to first-principles results we can compute the three stacking energies γ_{isf}, γ_{us}, and γ_{ut} with a reasonable amount of computational effort. Another important benefit to the simple expression for τ_a is that it gives us insight into the role of different material properties in controlling DT. For example, the reason for the low incidence of DT in Al compared to Cu is clear. Two ratios control τ_a through the two terms in the product in Eq. (4): γ_{isf}/γ_{us} and γ_{us}/γ_{ut}. The differences between Al and Cu in each ratio result in a 4% difference in τ_a, so both ratios contribute equally to the 8% difference in τ_a between Al and Cu. Thus, the low incidence of DT in Al is caused both by a high intrinsic SFE and a high unstable-twinning energy compared with the unstable-stacking energy.

Another result to come out of our calculations is that Pd should twin relatively easily. According to the values of τ in Table III, Pd should twin comparably to Cu or Pb, despite a significantly higher intrinsic SFE, closer to that of Al (see Table I). In fact, Pd's higher intrinsic SFE does lead to the γ_{isf}/γ_{us} term suppressing twinnability relative to Cu, but the γ_{us}/γ_{ut} term enhances it, leading to a net 2% enhancement of τ_a. Again, as in the case of Al, all three stacking energies are important for determining the twinnability of Pd. To our knowledge an experimental study of DT in bulk Pd has not been carried out. However, deformation twins have been observed in electrodeposited Pd.[24] The authors find that when electrodeposited Pd is thinned into TEM foils, a high density of deformation twins forms in the film. The large number of twins and the fact that they form at room temperature indi-

TABLE VIII. Literature values for stacking energies (mJ/m^2) and twinning stress (MPa) from first-principles (FP) calculations and experiment (expt). First-principles values labeled with an asterisk indicate unrelaxed energies.

Mat.	γ_{isf}^{expt}	γ_{isf}^{FP}	γ_{esf}^{expt}	γ_{esf}^{FP}	$2\gamma_t^{expt}$	$2\gamma_t^{FP}$	γ_{us}^{FP}	σ_T
Ag	16 (Ref. 29) 22 (Ref. 32) 21 (Ref. 34)	50 (Ref. 30) 46 (Ref. 16) 21* (Ref. 31) 33 (Ref. 18)		29* (Ref. 31) 38 (Ref. 18)	16 (Ref. 32)	28* (Ref. 31) 38 (Ref. 18)	190 (Ref. 30)	40-60 (Ref. 5) 48 (Ref. 33) 58-71 (Ref. 34) 63 (Ref. 4) 69-91 (Ref. 35)
Al	150 (Ref. 36) 166 (Ref. 32) 135 (Ref. 38) 200 (Ref. 42)	158 (Ref. 37) 170 (Ref. 30) 164 (Ref. 41) 164 (Ref. 16) 143 (Ref. 31) 154 (Ref. 39) 156 (Ref. 40) 161 (Ref. 43) 280 (Ref. 44) 126 (Ref. 45) 124 (Ref. 18) 160 (Ref. 47) 142 (Ref. 49) 140 (Ref. 48)	180 (Ref. 38)	147* (Ref. 31) 138 (Ref. 39) 138 (Ref. 40) 151 (Ref. 43) 260 (Ref. 44) 108 (Ref. 45) 118 (Ref. 18) 133 (Ref. 47) 130 (Ref. 48)	150 (Ref. 32) 150 (Ref. 38) 240 (Ref. 42)	146* (Ref. 31) 120 (Ref. 40) 148 (Ref. 43) 260 (Ref. 44) 108 (Ref. 45) 112 (Ref. 18) 118 (Ref. 46) 122 (Ref. 47) 110 (Ref. 49) 130 (Ref. 48)	175 (Ref. 37) 215 (Ref. 30) 224 (Ref. 41) 183 (Ref. 31)	
Au	33 (Ref. 50) 32 (Ref. 51) 45 (Ref. 32) 30 (Ref. 34)	44 (Ref. 18)		44 (Ref. 18)	30 (Ref. 32)	42 (Ref. 18)		80-100 (Ref. 5) 91-99 (Ref. 34)
Cu	45 (Ref. 52) 78 (Ref. 32) 35-45 (Ref. 55)	39 (Ref. 37) 49 (Ref. 54) 64 (Ref. 56) 51* (Ref. 31) 70 (Ref. 18)		54* (Ref. 31) 73 (Ref. 18)	48 (Ref. 32)	56* (Ref. 31) 72 (Ref. 18) 58 (Ref. 46)	158 (Ref. 37) 210 (Ref. 54)	40 (Ref. 53) 125-180 (Ref. 5) 140-158 (Ref. 55)
Ir	480 (Ref. 21) 300 (Ref. 32)	414 (Ref. 30) 534 (Ref. 18)		494 (Ref. 18)		486 (Ref. 18)	910 (Ref. 30)	1000 (Ref. 19)
Ni	 125 (Ref. 57) 128 (Ref. 32) 180-300 (Ref. 59)	183 (Ref. 54) 145 (Ref. 54) 182* (Ref. 31) 180 (Ref. 18)		175* (Ref. 31) 149 (Ref. 18)	86 (Ref. 32) 86 (Ref. 58)	174* (Ref. 31) 140 (Ref. 18)	350 (Ref. 54) 269 (Ref. 54)	300 (Ref. 5)
Pb	25 (Ref. 58)				20 (Ref. 59)			45-165 (Ref. 60)
Pd	175 (Ref. 32) 180 (Ref. 42)	176 (Ref. 31) 161 (Ref. 18)		178* (Ref. 31) 156 (Ref. 18)		178* (Ref. 31) 194 (Ref. 44) 152 (Ref. 18)	265 (Ref. 31)	
Pt	322 (Ref. 32)				322 (Ref. 32)			

rectly reinforce our claim that Pd is one of the more twinnable of the fcc metals.

V. CONCLUSIONS

We have presented TB calculations of stacking energies in fcc metals and used them to evaluate a theoretical predictor of twinnability, the tendency of a material to plastically deform by DT as opposed to dislocation-mediated slip. Using the NRL-TB method we evaluated the intrinsic SFE, unstable-stacking energy and unstable-twinning energy that control twinnability, as well as the extrinsic SFE and twin-boundary energy, in eight fcc metals. We find that the ranking of the metals in order of twinnability agrees with the experimental ranking, with Ag the most twinnable and Pt the least twinnable. An accurate approximation for the twinnability makes the calculation straightforward, and gives insight into the material properties that control twinnability. In particular, both the low incidence of DT in Al and the prediction of high twinnability for Pd can only be explained by differences in the intrinsic SFE combined with differences in the unstable-stacking energies. We hope that our prediction for DT in Pd will be investigated experimentally.

The measure for twinnability presented here is strictly ap-

plicable only to DT at zero temperature under quasistatic loading. Further work remains to extend this approach to finite temperatures, finite loading rates, and different crystal lattice structures, all of which are known experimentally to affect twinning.

Furthermore, the twinnability measure constitutes only an average qualitative measure for the inherent tendency of a material to twin. A more exact measure must account for the complexity inherent in materials and in the loading applied to them. From a theoretical standpoint, this could be achieved by incorporating the DT criterion into a crystal plasticity model that can then be used to predict the macroscopic response in a continuum plasticity simulation. Ideally, such analyses should be compared with direct atomistic molecular-dynamics or lattice-statics simulations. For example, one might simulate the plastic deformation near a crack tip or under a nanoindenter and compare the results with the predictions of crystal plasticity models. Atomistic simulations of this type would need to rely on new advances in coupling different computational techniques,[25–27] using an explicit TB description solely at the expected twinning-dislocation nucleation site. A direct simulation could reveal new atomic scale detail about the microscopic mechanisms, but would need to address the challenges of the required size of the TB region, the time scales for development of a

twinned region, and the difficulties in simulating a metallic system. For the foreseeable future combinations of analytical and numerical calculations, such as we presented here, and direct atomistic simulations will complement each other.

APPENDIX A: TIGHT-BINDING MODEL PARAMETERS

In Tables IV–VII we list the TB model parameters for Ag, Cu, Ir, and Pb, respectively.

APPENDIX B: EXPERIMENTAL AND FIRST-PRINCIPLES STACKING ENERGIES

In Table VIII we list a summary of previously published experimental and first-principles values for the intrinsic SFE, extrinsic SFE, twin-boundary energy, unstable-stacking energies, and twinning stress.

---

[1] See, for example, MRS Bull **26**(3), 2001 special issue on "Materials Research by Means of Multiscale Computer Simulation," edited by T.D. de la Rubia and V.V. Bulatov.

[2] J.P. Hirth and J. Lothe, *Theory of Dislocations* (McGraw Hill, New York, 1968).

[3] J.W. Christian and S. Mahajan, Prog. Mater. Sci. **39**, 1 (1995).

[4] A.T. English and G.Y. Chin, Acta Metall. **13**, 1013 (1965).

[5] M.A. Meyers, D.J. Benson, O. Vohringer, B.K. Kad, Q. Xue, and H.-H. Fu, Mater. Sci. Eng., A **322**, 194 (2002).

[6] J.A. Venables, in *Deformation Twinning*, edited by R.E. Reed-Hill (Gordon and Breach, New York, 1963), Vol. 25, pp. 77–111.

[7] S. Hai and E.B. Tadmor, Acta Mater. **51**, 117 (2003).

[8] M. Chen, E. Ma, K.J. Hemker, H. Sheng, Y. Wang, and X. Cheng, Science **300**, 1275 (2003).

[9] E.B. Tadmor and S. Hai, J. Mech. Phys. Solids **51**, 765 (2003).

[10] E.B. Tadmor and N. Bernstein (unpublished).

[11] R.E. Cohen, M.J. Mehl, and D.A. Papaconstantopoulos, Phys. Rev. B **50**, 14 694 (1994).

[12] M.J. Mehl and D.A. Papaconstantopoulos, Phys. Rev. B **54**, 4519 (1996).

[13] J.R. Rice, J. Mech. Phys. Solids **40**, 239 (1992).

[14] See, for example, the tabulated values in Appendix B.

[15] M.J. Mehl, B.M. Klein, and D.A. Papaconstantopoulos, in *Intermetallic Compounds*, edited by J.H. Westbrook and R.L. Fleischer (Wiley, New York, 1994), Vol. 1.

[16] M.J. Mehl, D.A. Papaconstantopoulos, N. Kioussis, and M. Herbranson, Phys. Rev. B **61**, 4894 (2000).

[17] W.H. Press, B.P. Flannery, S.A. Teukolsky, and W.T. Vetterling,

Numerical Recipes in C (Cambridge University Press, Cambridge, 1988).

[18] S. Crampin, K. Hampel, D.D. Vvedensky, and J.M. Maclaren, J. Mater. Res. **5**, 2107 (1990).

[19] O. Nishikawa and R.J. Walko, Acta Metall. **19**, 1163 (1971).

[20] P. Panfilov, V. Novgorodov, and G. Baturin, J. Mater. Sci. Lett. **11**, 229 (1992).

[21] R. Adamesku, S. Grebenkin, A. Yermakov, and P. Panfilov, J. Mater. Sci. Lett. **13**, 865 (1994).

[22] The error was computed using FP ratios of intrinsic SFE and unstable stacking energy from the same calculation.

[23] If we assume that the error in γ_{us}/γ_{ut} is comparable to that of γ_{isf}/γ_{us} then the error in $\sqrt{\gamma_{us}/\gamma_{ut}}$ will be about half that of γ_{isf}/γ_{us}. The reason for this is that the square-root operation increases the values of the parameters and reduces the relative difference between the TB and FP values. As an approximation we therefore neglect the error in $\sqrt{\gamma_{us}/\gamma_{ut}}$ relative to γ_{isf}/γ_{us}.

[24] L.A. Giannuzzi, P.R. Howell, H.W. Pickering, and W.R. Bitler, Scr. Metall. **23**, 1353 (1989).

[25] F.F. Abraham, J.Q. Broughton, N. Bernstein, and E. Kaxiras, Europhys. Lett. **44**, 783 (1998).

[26] N. Bernstein and D.W. Hess, Phys. Rev. Lett. **91**, 025501 (2003).

[27] S. Ogata, F. Shimojo, R.K. Kalia, A. Nakano, and P. Vashishta, Comput. Phys. Commun. **149**, 30 (2002).

[28] D.A. Papaconstantopoulos and M.J. Mehl, J. Phys.: Condens. Matter **15**, R413 (2003).

[29] H. Saka, Y. Sueki, and T. Imura, Philos. Mag. A **37**, 273 (1978).

[30] N. Kioussis, M. Herbranson, E. Collins, and M.E. Eberhart, Phys. Rev. Lett. **88**, 125501 (2002).

[31] J. Hartford, B. von Sydow, G. Wahnstrom, and B.I. Lundqvist, Phys. Rev. B **58**, 2487 (1998).

[32] L.E. Murr, *Interfacial Phenomena in Metals and Alloys* (Addison Wesley, Reading, 1975).

[33] B. Ramaswami, J. Appl. Phys. **36**, 2569 (1965).

[34] H. Suzuki and C.S. Barrett, Acta Metall. **6**, 156 (1958).

[35] M. Ahlers and P. Haasen, Z. Metallkd. **53**, 302 (1962).

[36] M.J. Mills and P. Stadelmann, Philos. Mag. A **60**, 355 (1989).

[37] S. Ogata, J. Li, and S. Yip, Science **298**, 807 (2002).

[38] R.E. Smallman and P.S. Dobson, Metall. Trans. **1**, 2383 (1970).

[39] Q.H. Jin, P.J. Wang, D.T. Ding, and D.S. Wang, Phys. Lett. A **174**, 437 (1993).

[40] B. Hammer, K.W. Jacobsen, V. Milman, and M.C. Payne, J. Phys.: Condens. Matter **4**, 10 453 (1992).

[41] G. Lu, N. Kioussis, V.V. Bulatov, and E. Kaxiras, Phys. Rev. B **62**, 3099 (2000).

[42] I.L. Dillamore and R.E. Smallman, Philos. Mag. **12**, 191 (1965).

[43] A.F. Wright, M.S. Daw, and C.Y. Fong, Philos. Mag. A **66**, 387 (1992).

[44] J.H. Xu, W. Lin, and A.J. Freeman, Phys. Rev. B **43**, 2018 (1991).

[45] P.J. Denteneer and J.M. Soler, J. Phys.: Condens. Matter **3**, 8777 (1991).

[46] J.M. MacLaren, S. Crampin, D.D. Vvedensky, and M.E. Eberhart, Phys. Rev. Lett. **63**, 2586 (1989).

[47] J.P. Simon, J. Phys. F: Met. Phys. **9**, 425 (1979).

[48] P. Wilkes and C.M. Sargent, Met. Sci. J. **6**, 216 (1972).

[49] J.F. Devlin and W. Bollmann, Phys. Status Solidi A **27**, K57 (1975).

[50] T.J. Balk and K.J. Hemker, Philos. Mag. A **81**, 1507 (2001).

[51] M.L. Jenkins, Philos. Mag. **26**, 747 (1972).

[52] C.B. Carter and I.L. Ray, Philos. Mag. **35**, 189 (1977).

[53] D. Weiner, Acta Metall. **20**, 1235 (1972).

[54] J.A. Zimmerman, H.J. Gao, and F.F. Abraham, Modell. Simul. Mater. Sci. Eng. **8**, 103 (2000).

[55] P.R. Thornton and T.E. Mitchell, Philos. Mag. **7**, 361 (1962).

[56] L.G. Wang and M. Sob, Phys. Rev. B **60**, 844 (1999).

[57] C.B. Carter and S.M. Holmes, Philos. Mag. **35**, 1161 (1977).

[58] R.P. Reed, Philos. Mag. **15**, 1051 (1967).

[59] G.F. Bolling, H.W. Wiedersich, and L.E. Hays, Acta Metall. **10**, 185 (1962).

[60] G.F. Bolling, K.W. Casey, and R.H. Richman, Philos. Mag. **12**, 1079 (1965).